Adaptive optics with combined optical coherence tomography and scanning laser ophthalmoscopy for in vivo mouse retina imaging

Pengfei Zhang, Daniel J. Wahl, Jacopo Mocci, Suman Manna, Ratheesh K. Meleppat, et al.

Pengfei Zhang, Daniel J. Wahl, Jacopo Mocci, Suman Manna, Ratheesh K. Meleppat, Stefano Bonora, Marinko V. Sarunic, Edward N. Pugh, Robert J. Zawadzki, "Adaptive optics with combined optical coherence tomography and scanning laser ophthalmoscopy for in vivo mouse retina imaging," Proc. SPIE 10474, Ophthalmic Technologies XXVIII, 1047427 (18 March 2018); doi: 10.1117/12.2288607

SPIE.

Event: SPIE BiOS, 2018, San Francisco, California, United States

Adaptive Optics with Combined Optical Coherence Tomography and Scanning Laser Ophthalmoscopy for *in vivo* mouse retina imaging

Pengfei Zhang[1], Daniel J. Wahl[2], Jacopo Mocci[3], Suman Manna[1], Ratheesh K. Meleppat[1], Stefano Bonora[3], Marinko V. Sarunic[2], Edward N. Pugh Jr. [1], and Robert J. Zawadzki[1,4*]

[1]UC Davis Eye-pod, Department of Cell Biology and Human Anatomy, University of California Davis, Davis, CA 95616

[2]Engineering Science, Simon Fraser University, Burnaby BC, V5A 1S6, Canada

[3]CNR-Institute for Photonics and Nanotechnology, Via Trasea 7, 35131, Padova, Italy

[4]UC Davis Eye Center, Dept. of Ophthalmology & Vision Science, University of California Davis, 4860 Y Street, Suite 2400, Sacramento, California 95817

*rjzawadzki@ucdavis.edu

ABSTRACT

Optical coherence tomography (OCT) and scanning laser ophthalmoscopy (SLO) are two state-of-the-art imaging technologies commonly used to study retina. Adaptive Optics (AO) methodologies enable high-fidelity correction of ocular aberrations, resulting in improved resolution and sensitivity for both SLO and OCT systems. Here we present work integrating OCT into a previously described mouse retinal AO-SLO system, allowing simultaneous reflectance and fluorescence imaging. The new system allows simultaneous data acquisition of AO-SLO and AO-OCT, facilitating registration and comparison of data from both modalities. The system has data acquisition speed of 200 kHz A-scans/pixel, and high volumetric resolution.

Keywords: Adaptive Optics; Scanning Laser Ophthalmoscopy; Optical Coherence Tomography; Retinal Imaging; Multimodal System

1. INTRODUCTION

The mouse retina is an important model in vision science and ophthalmic research. It is also an optically accessible extension of the brain and affords the unique opportunity to non-invasively visualize changes associated with neurodegenerative disorders and vascular alterations of neural tissue. Scanning Laser Ophthalmoscopy (SLO) [1-3] and Optical Coherence Tomography (OCT) [4-9] are two common in vivo retinal imaging modalities, which have been successfully applied to monitor structural changes in the retina of living animals, enabling experiments that map changes in retinal reflectivity and morphology over seconds, days, weeks and months. The combination of these modalities provides a wealth of complementary information, as showcased by our previous work [10-14].

Most retinal imaging system employs the eye's natural optics as the imaging objective. Due to optical aberrations of the lens and cornea it is impossible to use the full pupil of the eye while maintaining diffraction-limited performance. Consequently, both SLO and OCT typically use scanning beams whose width is a small fraction of the pupil diameter[15, 16]. The trade-off is a relatively low lateral resolution for both systems. However, high resolution imaging is desirable to better visualize the cellular structures and understand the cellular level processes in the living retina. Adaptive Optics (AO) improves the system's optical performance by compensating for the ocular aberrations using wavefront shaping components (deformable mirror or spatial light modulators), allowing us to use the maximum numerical aperture of the imaging objective (mouse eye), and thus the maximum available resolution [17-21].

Here we report our work on integrating OCT into our previously reported AO-SLO system [22] for in vivo mouse retina imaging. The manuscript was organized as following: the system design is first described. Then, the OCT performance is given by calibrating its spectrometer. Further, the AO-SLO-OCT is demonstrated on a model eye. After

Ophthalmic Technologies XXVIII, edited by Fabrice Manns, Per G. Söderberg, Arthur Ho, Proc. of SPIE
Vol. 10474, 1047427 · © 2018 SPIE · CCC code: 1605-7422/18/$18 · doi: 10.1117/12.2288607

that, a mouse retina was imaged to show the AO-OCT control of axial position, thanks to highly localized enhancement in retinal intensity. Finally, several key points about system construction were discussed followed by brief conclusions.

2. SYSTEM DESCRIPTION

In our previous study, an *in vivo* mouse retinal AO-SLO imaging system was built and successfully applied to study cellular morphology *in vivo* [22]. Here we briefly report on changes to system components made since then. We recently upgraded our Shack-Hartmann wavefront sensor (SHWS) [23] and redesigned the three detection channels of the SLO system to optimize the AO system performance, as shown in Fig. 1: The wavefront sensor was set on-axis of the system entrance pupil at the position conjugate to the pupil plane to ensure precise wavefront measurement. The dichroic mirror was upgraded to an ultra-flat dichroic (Chroma) to minimize the aberrations introduced during reflection of blue reflectance and fluorescence channels. The AO controller was upgraded to new version that can measure and correct aberrations at 100+ Hz using high spatial sampling of the pupil (40 x 40 lenslets on 2 x 2 mm^2 pupil). Fig 1 also shows changes introduced to the system to allow integration of OCT into this AO-SLO: the light for wavefront sensing and SLO imaging was introduced into the system by beamsplitter BS1, then the light pass through a cascade of 4f telescopes (all spherical mirrors except the last lens) into the mouse eye, ensuring optical conjugation of the mouse pupil with the Deformable Mirror, the X- and Y-Scanners, Imaging objective lens, and SH-WFS lenslet. A short-pass ultra-flat dichroic mirror (DM1, t750spxr-xt-uf, Chroma) was used to introduce OCT light into AO-SLO system that also acts as the sample arm of the AO-OCT system. Separate reference arm matching the lengths of the AO-OCT sample arm (~11.5 meters long) was built. A supercontinuum laser (NKT) served as the OCT light source. The OCT light was centered at 800 nm with 65 nm FWHM bandwidth which provides about 6.3 µm axial resolution in air. A spectrometer comprising of 1200 lines/mm diffraction grating (Wasatch Photonics 1200lpmm at 840 nm), a 4096 pixels line scan camera (Basler SPL4096-140km) and imaging optics was built in house. The combined system offered a 200 kHz A-scan rate for 1024 pixels acquired by line scan camera.

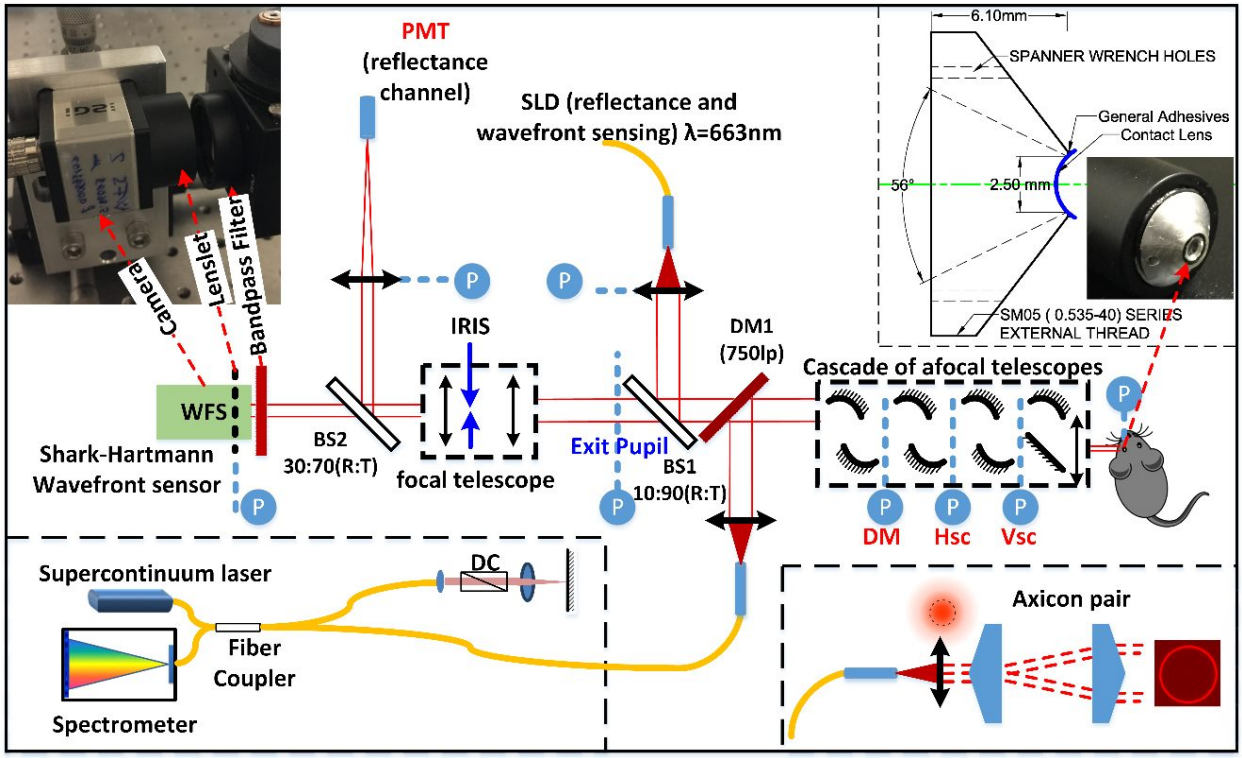

Fig.1. Schematic of the multi-modal AO-SLO-OCT mouse retinal imaging system: BS# - beam splitter; DC - dispersion compensation; DM1- dichroic mirror; DM - deformable mirror; PMT - photomultiplier tube; P (circled in blue and marked with blue dashed line) - optical planes conjugate with the pupil; SLD - superluminescent diode; Hsc/Vsc - horizontal/vertical scanner.

The Shack-Hartmann wavefront sensor-based AO systems are usually very sensitive to back-reflections from the optical elements. In our current system, there is back-reflection from the last lens of the cascade of focal telescopes, and from the contact lens and a mouse cornea. To eliminate these reflections, a small aperture stop (~2 mm in diameter) was placed right after the collimator of the SLD light source to create a dark region in the center of the beam used for wavefront sensing. As an alternate approach we used an axicon lens pair (Asphericon) to create annular/circular collimated illumination light, as shown in bottom right corner blue dashed line box. The axicon lens pair converts the Gaussian beam profile into Bessel beam. The ring diameter is adjusted by moving the second axicon. This configuration also allows reduction of spherical aberration, and extension of the depth of focus of wavefront beacon.

3. RESULTS

3.1 Sensitivity fall-off and axial resolution

The spectrum of the light source was measured by our custom build spectrometer. As shown in Fig. 2 (a), it has a ~65 nm FWHM bandwidth. The spectrometer mapping of pixels to wavenumbers (spectral mapping) was calibrated as shown in Fig. 2 (b). Then, we measured spectrometer sensitivity fall-off be placing sample mirror at different depths, as shown in Fig. 2 (c). Fig. 2 (d) shows FWHM axial resolution at different depth. The averaged resolution within 1 mm depth is about 6.3 μm in air, which is roughly 4.7 μm in tissue by assuming a tissue refraction index of 1.33.

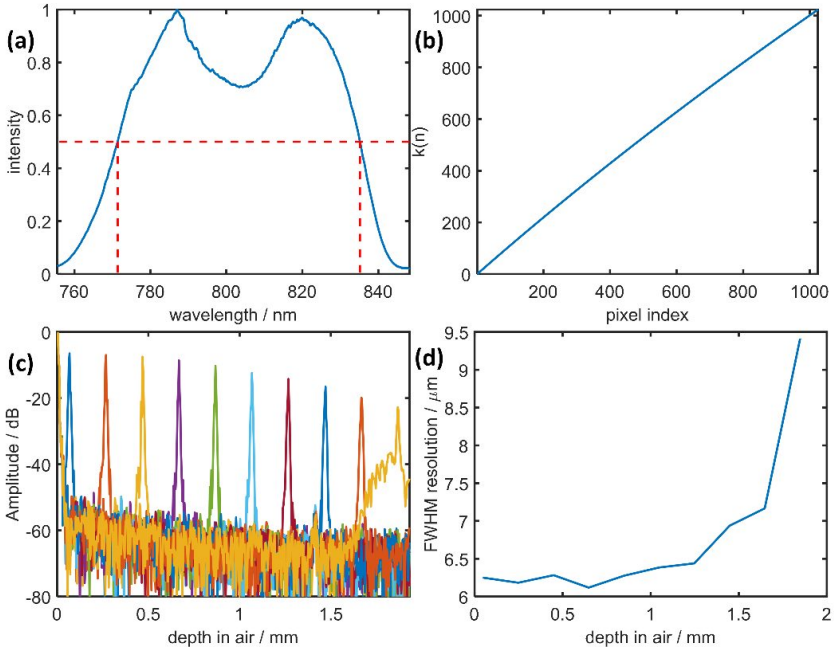

Fig.2. OCT spectrometer calibration. (a): normalized reference arm spectrum measured by the custom spectrometer; (b): spectral mapping of the spectrometer: wavenumber k(n) versus pixel index; (c): Sensitivity fall-off as a function of depth; (d): FWHM resolution at different depths.

3.2 Model eye AO-OCT testing

First, a model eye with a 100mm achromatic lens as the objective and a print paper as the retina was used to test our combined AO-SLO-OCT system. The images of SLO, OCT enface projection and OCT B-scans before and after AO correction are shown in Fig. 3, which is clearly showcases the overall enhancement of AO in terms of image intensity. The OCT enface intensity projection is also shown to visualize improvement in image sharpness after AO correction. We further quantify the improvement in image quality by comparing changes in wavefront RMS error (Fig. 4 (a) from 0.3μm to 0.03μm), Histogram changes (Fig. 4 (b) and (c) are for SLO and OCT enface projection, respectively). Fig. 4 (d) shows the OCT line profile (averaged from 50 A-scans centered at B-scan shown in Fig. 3) changes. The OCT A-scan line intensity profile (linear to the sample arm light amplitude) increases about 2.3 times after AO correction.

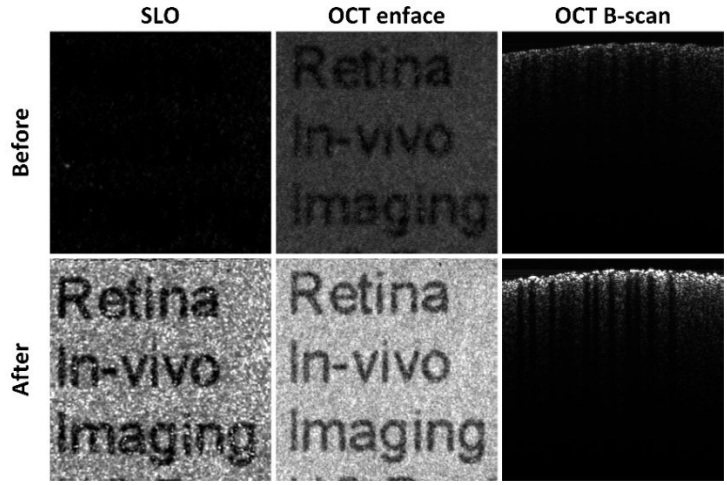

Fig.3. Image comparisons of SLO, OCT enface projection and OCT B-scan before and after AO correction for a model eye.

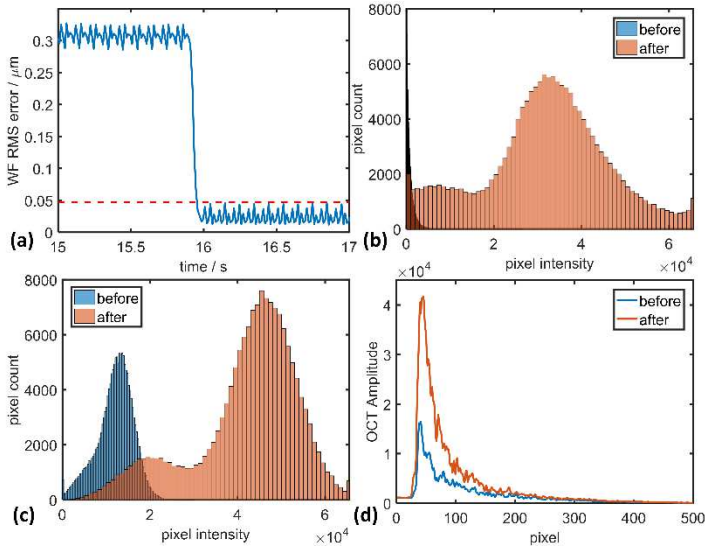

Fig.4. Quantified comparisons for, (a) Wavefront RMS error changes, (b) SLO image histogram, (c) OCT enface projection histogram changes. (d) OCT line intensity profile changes, before and after AO correction for the images shown in Fig. 3.

3.3 In-vivo mouse retinal AO-OCT imaging

The AO-OCT sub-system was tested by imaging a pigmented mouse retina in-vivo to demonstrate its capability. Due to the chromatic aberration, the AO-OCT beam (centered at 800nm) was naturally focused on the Choroid layer, as shown in Fig. 5 (a), only RPE and Choroid layers are clearly visible in AO-OCT B-scans (linear to sample arm light amplitude). After closing loop, the A-scan intensity profiles (averaged from the center 100 A-scans from each B-scan) clearly show the signal enhancement around RPE-Choroid layers, and all the rest of the retina layers are not enhanced. To visualize other layers, we needed to shift the focus to the layer of interest. There are two ways to shift the focus in our system, one is by adding defocus on the deformable mirror, and the other way is to move the OCT sample arm fiber tip position further from the collimating lens. Here we tested the second way, as demonstrated by Fig. 5. It is worth to note that: when the light focuses on IS/OS layer, there is an additional peak that appear in the axial intensity profile, as indicated by the blue arrow shown in Fig. 5 (c), which might correspond to the cone outer segment tips; when the light focus on ONL layer (pointed by purple arrow in Fig. 5 (g)), it becomes more visible than adjacent plexiform layers which is not usual in normal OCT images.

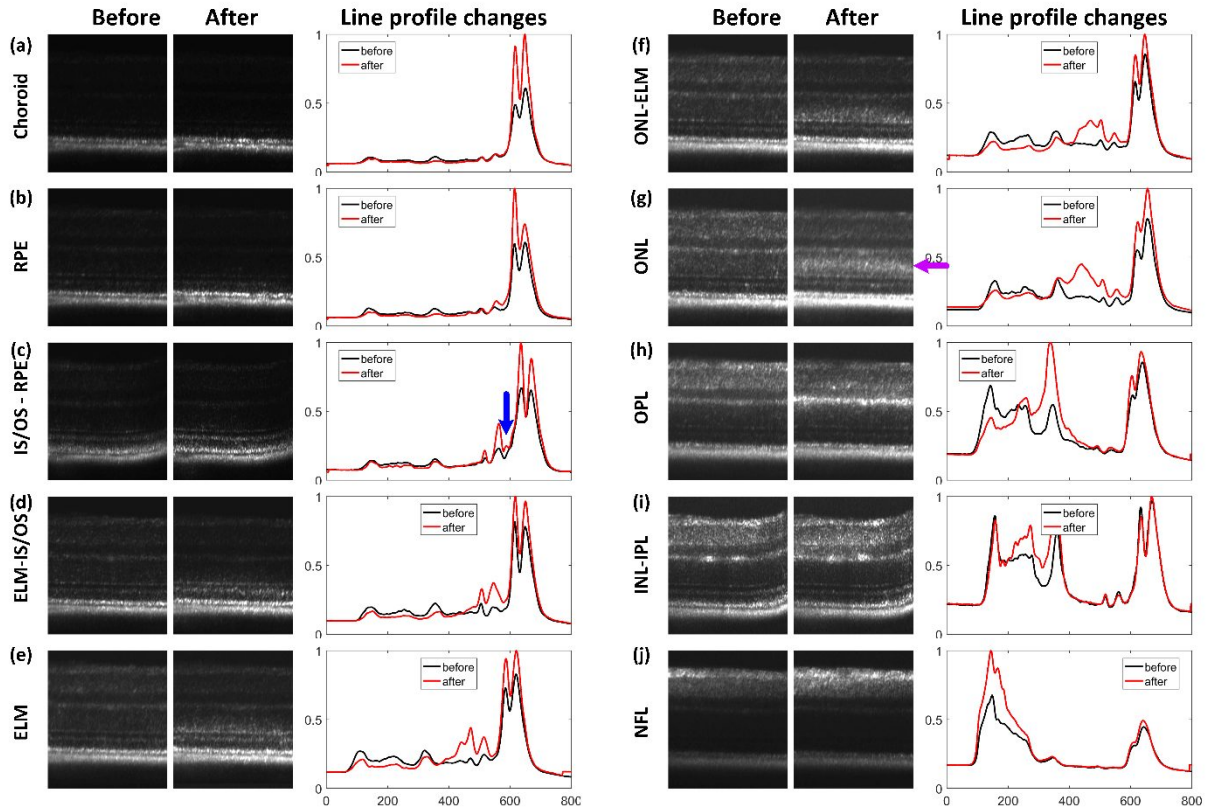

Fig.5. In vivo mouse retinal AO-OCT B-scan images showing the localization of the focal plane in our AO-OCT system. The B-scans show the improvement in image intensity only within very limited depth after AO correction due to relatively high NA of the mouse eye and corresponding confocal depth of focus; the line profile changes show the OCT signal changes (proportional to the sample light amplitude). RPE: retinal pigment epithelium; IS/OS: inner segment /outer segment of photoreceptors; ELM: external limiting membrane; ONL: outer nuclear layer; OPL: outer plexiform layer; IPL: inner plexiform layer; INL: inner nuclear layer; NFL: nerve fiber layer.

4. DISCUSSION

4.1 Dispersion compensation for broadband light source

The first difficulty we met during our system development was the dispersion compensation of OCT signal for broadband light source. In most OCT systems the differences in dispersion between sample and reference arm are usually keep to the minimum by using the same thickness of the dispersive materials in sample and reference arm (hardware dispersion compensation) and residual unmatched dispersion is compensated in OCT signal postprocessing by adding dispersive phase component to the spectral fringe before Fourier transform [24]. Since OCT was added to our existing AO-SLO system, we interfaced the OCT sample beam into AO-SLO system using reflection mode with dichroic mirror, as shown in Fig. 6 (a) green dashed line, not the preferred transmission mode (Fig. 6 (a) gray dashed line): To compensate the dispersion introduced by reflection of dichroic mirror in the sample arm we used another dichroic mirror in the reference arm. Although two identical ultra-flat dichroic mirrors were used to match the dispersion between reference arm and sample arm, the residual dispersion couldn't be matched using standard software dispersion compensation: Fig. 6 (b) shows the best PSFs from a mirror using different bandwidth of light source (Their spectra were shown in Fig. 6 (c) and (d) with red curves). The PSF from broadband (190nm bandwidth) light source has very broad and complex PSF if compared to narrowband (40nm bandwidth) light source, and their theoretical PSFs. This illustrates our inability to properly matched dispersion in this configuration and would result in image artifacts and blurring in the OCT images. The reason for this behavior is group delay dispersion (GDD)[25] introduced by the dichroic mirrors. Fig. 7 (c) and (d) plot its

GDD for s- / p- polarized light, which shows a huge spike in GDD around 850 nm. This narrowed down the useful bandwidth for our light source. To avoid this GDD anomaly we decided to limit our light source spectrum from 760nm to 840nm (Note that the dichroic is a 750nm short pass filter). Unfortunately this lowers axial resolution of our OCT system, however due to limited spectral range we could run our OCT detection spectrometer twice faster (200 kHz) and additionally limit the effect of chromatic aberration both transverse and longitudinal (LCA)[26]. We had two light sources that could operate in this spectral range an SLD with 40nm FWHM spectral bandwidth and an NKT source with tunable filter. We decided to use NKT source in our experiments because it can offer ~25nm broader bandwidth of light and three times more power.

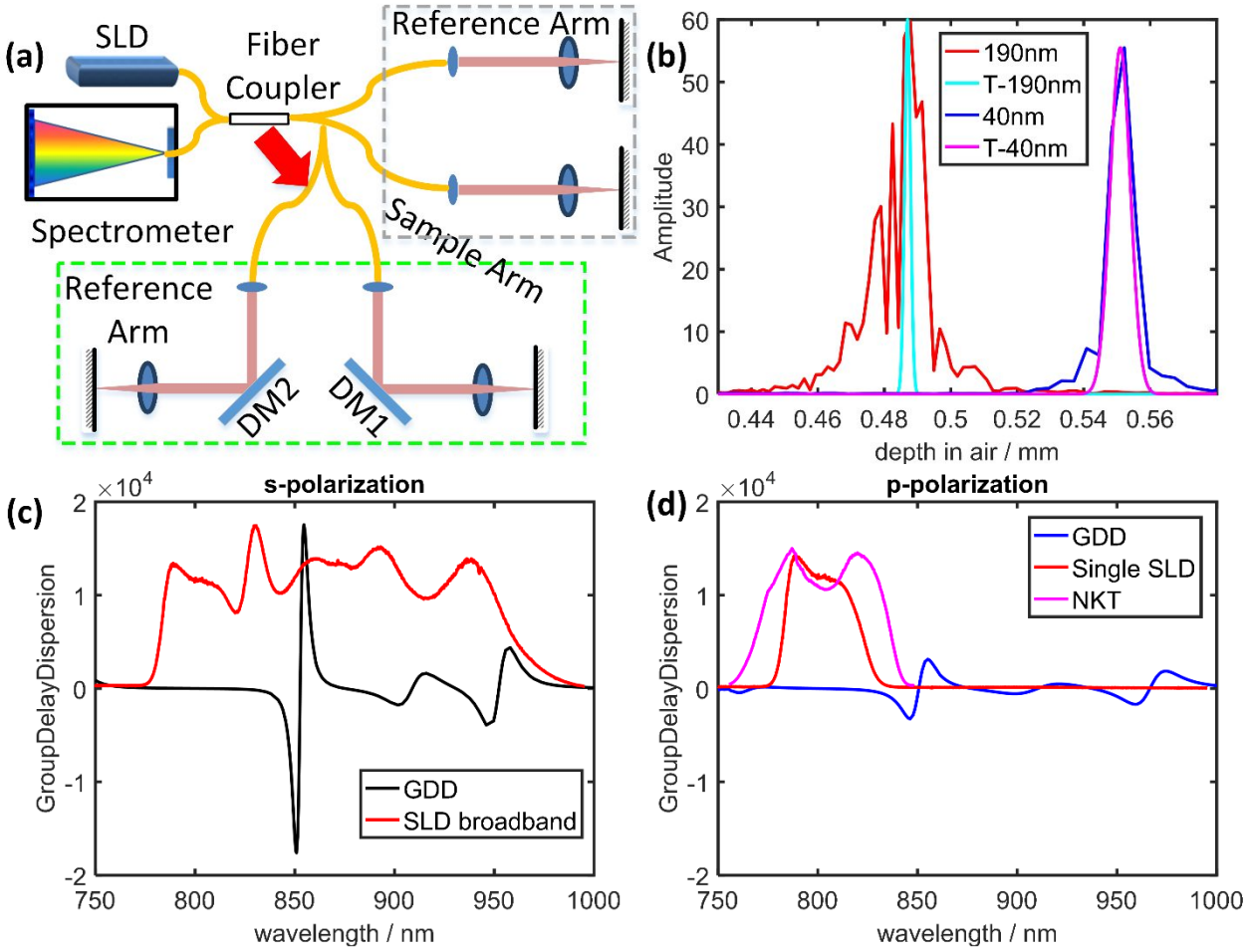

Fig.6. Group Delay Dispersion introduced by reflection from an ultra-flat Dichroic mirror limits the useful spectral range of the OCT system, (a) simplified OCT configuration sketch of our system (Transmission mode: gray dashed line box; Reflection mode: green dashed line box; DM: dichroic mirror); (b) Axial PSF for light sources with different bandwidth: 190nm centered at 870nm and 40nm centered at 800nm, T: Theoretical PSF; (c) group delay dispersion for p-polarization light, the red curve shows the broadband SLD light source spectrum; (d) group delay dispersion for s-polarization light, the red and pink curves show the spectrum of two light sources: single SLD and filtered NKT supercontinuum laser, respectively.

4.2 Comparison between NKT and SLD light source

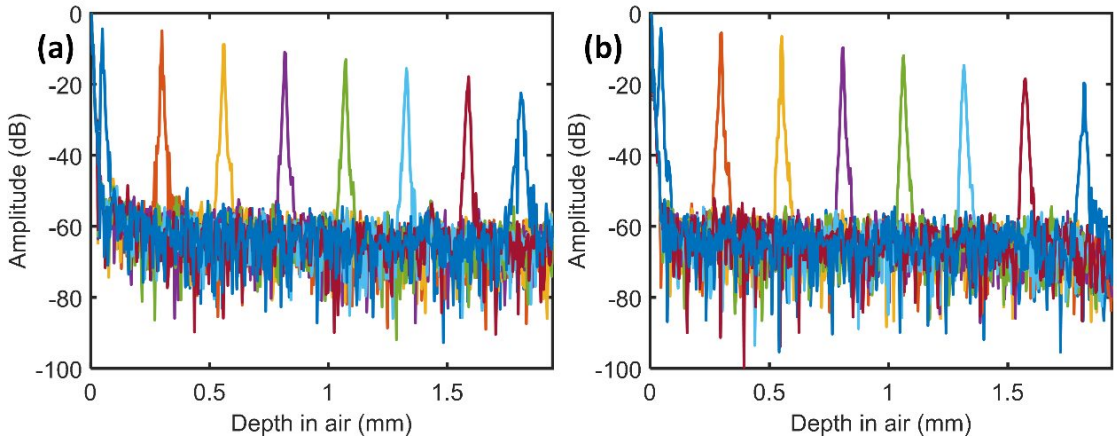

Fig.7. Sensitivity fall-off comparison between (a) NKT supercountinuum and (b) Superlum SLD light source in our OCT system.

We tested the performance of our OCT spectrometer for these two light sources (NKT supercountinuum and Superlum single SLD, spectrum shown in Fig. 6 (d)) in our OCT system by measuring the sensitivity roll-off, as shown in Fig. 7. Both light sources offer very similar dynamic range and noise level.

4.3 Aberrations introduced by axicon pair

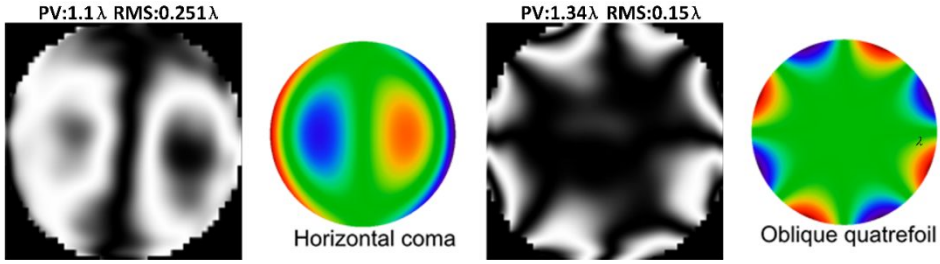

Fig.8. Two examples of aberration introduced by misaligned axicon pair. Left is coma, right one is Quatrefoil.

The axicon pair in our system was introduced into WFS beacon beam to reduce the back-reflection from the mouse cornea / contact lens (by creating ring intensity profile of that beam). Additionally, this results in creating Bessel beam on the retina what may benefit AO by the extending depth range of focus. We want to point out that while this is very useful it is also very sensitive to proper alignment of axicons. Fig. 8 shows two examples of the aberration introduced by not properly aligned axicon pair, measured by our wavefront sensor after application of wavfront sensorless AO correction using the intensity of the image created by the same light [27, 28].

5. CONCLUSION

A multimodal in-vivo mouse retina imaging system was developed by combing OCT into AO-SLO system to create an AO-SLO-OCT system. The system design, performance, and example high-resolution images acquired from mouse retina in vivo were presented. Several important points that were observed during the system development were discussed as well. We plan to use this system in the future for simultaneous AO-SLO/AO-OCT data acquisition in the living mouse eye and perform studies similar to our non AO SLO/OCT system [12]. In particular, we will evaluate the ability of the system to image the mouse photoreceptor mosaic, and plan to use the system to perform optophysiology of mouse cones, as we have for rods [14]. We also intend to use the system for simultaneous visualization of the ganglion cell bodies by AO-OCT using motility in the nuclei as contrast [21] and by AO-SLO using fluorescently labeled cells.

ACKNOWLEDGEMENT

Authors would like to acknowledge their funding sources: NSF I/UCRC CBSS Grant, NIH grants EY026556, and EY012576 (NEI Core Grant). This work was partially supported by Barr Retina Research Foundation gift to UC Davis Department of Ophthalmology.

REFERENCES

[1] R. H. Webb, and G. W. Hughes, "Scanning laser ophthalmoscope," Ieee Transactions on Biomedical Engineering, 28(7), 488-492 (1981).

[2] M. W. Seeliger, S. C. Beck, N. Pereyra-Munoz *et al.*, "In vivo confocal imaging of the retina in animal models using scanning laser ophthalmoscopy," Vision Research, 45(28), 3512-3519 (2005).

[3] M. Paques, M. Sirnonutti, M. J. Roux *et al.*, "High resolution fundus imaging by confocal scanning laser ophthalmoscopy in the mouse," Vision Research, 46(8-9), 1336-1345 (2006).

[4] D. Huang, E. Swanson, C. Lin *et al.*, "Optical coherence tomography," Science, 254(5035), 1178-1181 (1991).

[5] W. Drexler, U. Morgner, R. K. Ghanta *et al.*, "Ultrahigh-resolution ophthalmic optical coherence tomography," Nature Medicine, 7, 502 (2001).

[6] R. Leitgeb, C. K. Hitzenberger, and A. F. Fercher, "Performance of fourier domain vs. time domain optical coherence tomography," Optics Express, 11(8), 889-894 (2003).

[7] J. G. Fujimoto, "Optical coherence tomography for ultrahigh resolution in vivo imaging," Nature Biotechnology, 21, 1361 (2003).

[8] W. Drexler, and J. G. Fujimoto, "State-of-the-art retinal optical coherence tomography," Progress in Retinal and Eye Research, 27(1), 45-88 (2008).

[9] E. S. Levine, A. Zam, P. Zhang *et al.*, "Rapid light-induced activation of retinal microglia in mice lacking Arrestin-1," Vision Research, 102, 71-79 (2014).

[10] P. F. Zhang, A. Zam, E. N. Pugh *et al.*, "Evaluation of state-of-the-art imaging systems for in vivo monitoring of retinal structure in mice: current capabilities and limitations," Proceedings of SPIE. 8930.

[11] P. F. Zhang, A. Zam, Y. Jian *et al.*, "Multispectral scanning laser ophthalmoscopy combined with optical coherence tomography for simultaneous in vivo mouse retinal imaging," Ophthalmic Technologies XXV. 9307, 93070H

[12] P. F. Zhang, A. Zam, Y. F. Jian *et al.*, "In vivo wide-field multispectral scanning laser ophthalmoscopy-optical coherence tomography mouse retinal imager: longitudinal imaging of ganglion cells, microglia, and Muller glia, and mapping of the mouse retinal and choroidal vasculature," Journal of Biomedical Optics, 20(12), (2015).

[13] P. Zhang, M. Goswami, R. J. Zawadzki *et al.*, "The Photosensitivity of Rhodopsin Bleaching and Light-Induced Increases of Fundus Reflectance in Mice Measured In Vivo With Scanning Laser Ophthalmoscopy," Investigative Ophthalmology & Visual Science, 57(8), 3650-3664 (2016).

[14] P. Zhang, R. J. Zawadzki, M. Goswami *et al.*, "In vivo optophysiology reveals that G-protein activation triggers osmotic swelling and increased light scattering of rod photoreceptors," Proceedings of the National Academy of Sciences, (2017).

[15] Y. Zhang, and A. Roorda, "Evaluating the lateral resolution of the adaptive optics scanning laser ophthalmoscope," Journal of biomedical optics, 11(1), 014002-014002 (2006).

[16] P. F. Zhang, M. Goswami, A. Zam *et al.*, "Effect of scanning beam size on the lateral resolution of mouse retinal imaging with SLO," Optics Letters, 40(24), 5830-5833 (2015).

[17] R. J. Zawadzki, S. M. Jones, S. Pilli *et al.*, "Integrated adaptive optics optical coherence tomography and adaptive optics scanning laser ophthalmoscope system for simultaneous cellular resolution in vivo retinal imaging," Biomedical Optics Express, 2(6), 1674-1686 (2011).

[18] Y. Geng, A. Dubra, L. Yin *et al.*, "Adaptive optics retinal imaging in the living mouse eye," Biomedical Optics Express, 3(4), 715-734 (2012).

[19] S. Bonora, Y. F. Jian, P. F. Zhang *et al.*, "Wavefront correction and high-resolution in vivo OCT imaging with an objective integrated multi-actuator adaptive lens," Optics Express, 23(17), 21931-21941 (2015).

[20] E. A. Rossi, C. E. Granger, R. Sharma *et al.*, "Imaging individual neurons in the retinal ganglion cell layer of the living eye," Proceedings of the National Academy of Sciences, 114(3), 586-591 (2017).

[21] Z. Liu, K. Kurokawa, F. Zhang *et al.*, "Imaging and quantifying ganglion cells and other transparent neurons in the living human retina," Proceedings of the National Academy of Sciences, (2017).
[22] R. J. Zawadzki, P. Zhang, A. Zam *et al.*, "Adaptive-optics SLO imaging combined with widefield OCT and SLO enables precise 3D localization of fluorescent cells in the mouse retina," Biomedical Optics Express, 6(6), 2191-2210 (2015).
[23] J. Mocci, M. Quintavalla, C. Trestino *et al.*, "A multi-platform CPU-based architecture for cost-effective adaptive optics systems," IEEE Transactions on Industrial Informatics, PP(99), 1-1 (2018).
[24] M. Wojtkowski, V. J. Srinivasan, T. H. Ko *et al.*, "Ultrahigh-resolution, high-speed, Fourier domain optical coherence tomography and methods for dispersion compensation," Optics Express, 12(11), 2404-2422 (2004).
[25] J. B. Guild, C. Xu, and W. W. Webb, "Measurement of group delay dispersion of high numerical aperture objective lenses using two-photon excited fluorescence," Applied Optics, 36(1), 397-401 (1997).
[26] R. J. Zawadzki, B. Cense, Y. Zhang *et al.*, "Ultrahigh-resolution optical coherence tomography with monochromatic and chromatic aberration correction," Optics Express, 16(11), 8126-8143 (2008).
[27] Y. F. Jian, J. Xu, M. A. Gradowski *et al.*, "Wavefront sensorless adaptive optics optical coherence tomography for in vivo retinal imaging in mice," Biomedical Optics Express, 5(2), 547-559 (2014).
[28] D. J. Wahl, Y. Jian, S. Bonora *et al.*, "Wavefront sensorless adaptive optics fluorescence biomicroscope for in vivo retinal imaging in mice," Biomedical Optics Express, 7(1), 1-12 (2016).